Broadband low-frequency sound transmission loss improvement of double walls with Helmholtz resonators

F. Langfeldt[a,*], H. Hoppen[a], W. Gleine[a]

[a] *Department of Automotive and Aeronautical Engineering, Hamburg University of Applied Sciences, Berliner Tor 7a, D–20099 Hamburg, Germany*

Abstract

Helmholtz resonators are commonly used as narrowband sound absorbers in room acoustics applications. Previous research has shown that Helmholtz resonators can also be used to improve the sound transmission loss of double walls. The focus of this paper is the broadband improvement of the transmission loss of double walls in the low frequency region by tuning the Helmholtz resonators inside the cavity to frequencies lower or higher than the mass-air-mass resonance frequency of the double wall. A new analytical model using the effective material parameters (bulk modulus and density) of a fluid volume containing Helmholtz resonators is developed to describe the vibro-acoustic behavior of double walls with Helmholtz resonators. Using this model it can be shown that by tuning the Helmholtz resonators properly, the mass-air-mass resonance frequency of the unmodified double wall can be shifted significantly, leading to an improvement of the transmission loss of the double wall roughly between the mass-air-mass resonance frequency and the resonance frequency of the resonators. This improvement, however, comes along with a decrease of the transmission loss at high frequencies due to a decoupling of the Helmholtz resonators which is also covered by the proposed analytical model. Parametric studies are performed to identify relevant design parameters to optimize the transmission loss improvement by the Helmholtz resonators. Finally, experimental results of different double wall designs with integrated Helmholtz resonators are presented to validate the proposed analytical model and demonstrate the effectiveness under diffuse field incidence.

Keywords: resonance frequency, filling ratio, effective bulk modulus, effective density, analytical model, sound intensity measurement

1. Introduction

Compared to a single wall with the same mass, double wall partitions exhibit a considerably improved sound insulation performance for frequencies above the so-called mass-air-mass resonance frequency f_0 [1]. At lower frequencies, the sound transmission loss (STL) of a double wall is identical to that of a single wall with the same mass and for frequencies close to f_0 the STL can be greatly reduced due to the resonant behavior

*Corresponding author
Email address: Felix.Langfeldt@haw-hamburg.de (F. Langfeldt)

©2020. This manuscript version is made available under the CC-BY-NC-ND 4.0 license.
http://creativecommons.org/licenses/by-nc-nd/4.0/

Please cite as: Langfeldt, F., Hoppen, H., and W. Gleine. Broadband low-frequency sound transmission loss improvement of double walls with Helmholtz resonators. *Journal of Sound and Vibration* 476 (2020): 115309.
https://doi.org/10.1016/j.jsv.2020.115309

Accepted Manuscript

of the system. In many practical applications in noise control it is therefore desirable to design double wall partitions with a mass-air-mass resonance frequency that is below the frequency range of interest.

In the case of normal incidence, the mass-air-mass resonance frequency is given by [1]

$$f_0 = \frac{1}{2\pi}\sqrt{\frac{K}{H}\left(\frac{1}{m_1''} + \frac{1}{m_2''}\right)}, \tag{1}$$

where K is the bulk modulus of the fluid between the walls, H is the wall spacing, and m_1'' and m_2'' are the surface mass densities of the walls. From Eq. (1) it becomes clear that f_0 can be reduced by increasing the wall spacing (thus reducing the stiffness of the air layer between the walls) or by increasing the wall masses. Another possible (but less common) approach for this is to use a different fluid with a smaller bulk modulus (e.g. low pressure air or a near vacuum) in the gap between the walls.

In some practical applications these design changes for reducing the mass-air-mass resonance frequency of a double wall cannot be realized due to strict non-acoustic requirements. One particular example for this is the side wall of an aircraft cabin which is highly constrained in terms of mass and wall thickness, which is reduced between the fuselage frames to maximize passenger space. Consequently, there is a high demand for improving the STL of double walls at frequencies near or below f_0 without significantly changing the mass, wall spacing, and fluid between the walls.

A lot of research has been put into finding new technological solutions for this demand. For example, the STL of a double wall could be significantly improved at the mass-air-mass resonance by adding micro-resonators to the walls with their resonance frequencies specifically tuned to f_0 [2]. In Ref. [3], layers of so-called membrane-type acoustic metamaterials were placed in between the walls of a double wall partition to achieve considerably improved STL values at the anti-resonance frequencies of the metamaterials. By adding Helmholtz resonators to the cavity of a double wall, significant STL enhancement can also be achieved around the resonance frequencies of the embedded resonators [4–6]. This particular concept has been studied extensively and it has even been tested successfully inside the sidewall of a real aircraft structure [7]. Apart from these purely passive approaches, a wide range of investigations on the active control of noise transmission through double walls can be found in the literature (e.g. [8, 9]).

To the knowledge of the authors, all of the currently published studies of Helmholtz resonators inside a double wall focus on the more or less narrowband STL improvement at the Helmholtz resonance frequency. However, as Mason and Fahy [4] pointed out, if the Helmholtz resonators are tuned slightly above the mass-air-mass resonance frequency, the STL improvement can be quite broadband. So far, this phenomenon has not been explained on a physical basis and it was not exploited to achieve broadband STL improvements using Helmholtz resonators inside double walls. This paper aims at filling this gap. It will be shown that the mass-air-mass resonance frequency f_0 can be reduced significantly by including acoustic resonators inside a double wall. This way, the mass-air-mass resonance frequency f_0 can be reduced even if all other parameters of Eq. (1) like the wall spacing, wall masses (assuming that the Helmholtz resonators are an integral part of

Accepted Manuscript

the walls), and the cavity fluid are not changed. This results in improvements of the double wall STL which can be very large and broadband, if the resonators are designed properly.

In the past, other efforts have been made to achieve improved broadband noise insulation compared to conventional noise reduction techniques. For example, Helmholtz resonators were also successfully applied to reduce the sound pressure level inside the payload fairing of launch vehicles. The broadband noise reduction was achieved using a horn-like neck shape of the resonator to cause high absorption at low frequencies, while at higher frequencies the absorption was generated by porous materials surrounding the resonators [10]. This approach differs mainly in two aspects from the double wall with integrated Helmholtz resonators studied here: First, the Helmholtz resonators in the payload faring are designed to achieve high absorption in order to dampen the sound pressure levels occurring inside the comparatively small volume inside the fairing. The purpose of the double wall, on the other hand, is to reduce the transmission of sound by generating a high impedance mismatch. Second, the horn-shaped Helmholtz resonators exhibit the best absorption coefficients at very large sound pressure levels (> 130 dB), owing to non-linear effects at the orifice [11]. The double wall with Helmholtz resonators investigated in this paper, on the other hand, are applicable in the linear regime. Another approach to achieve broadband noise reduction improvement is to use optimally tuned dynamic vibration absorbers in order to reduce the vibrations of a structure over a broad frequency range [12, 13]. Estève and Johnson [14] investigated the effect of both optimally tuned dynamic vibration absorbers and Helmholtz resonators on the reduction of sound transmitted into a cylindrical shell. Their results show that the dynamic vibration absorbers can be used to reduce the sound transmission at structural resonances, while the Helmholtz resonators yield a more broadband effect due to the damping of acoustic resonances inside the cavity (similar to the payload fairing). Recently, sandwich panels with embedded acoustic metamaterials have been proposed to obtain broadband STL improvements compared to the mass-law sound transmission loss of a wall with the same surface mass density [15]. These type of metamaterial sandwich panels, however, have only been demonstrated using small-scale samples inside the impedance tube. This arrangement is strongly affected by the stiffness induced by the clamped boundaries, particularly at low frequencies, and the performance of this metamaterial is expected to be greatly diminished in large-scale specimens [16].

The paper is structured as follows: An analytical model is derived in Section 2 which provides a simple expression for calculating the effective bulk modulus of a fluid volume with Helmholtz resonators. This model is validated using impedance tube measurements and then applied to calculate the mass-air-mass resonance frequency and STL of double walls with Helmholtz resonators between the walls. In Section 3, parameter studies are performed to investigate how the shifting of the mass-air-mass resonance frequency by using Helmholtz resonators can be exploited to achieve broadband improvement of the double wall STL. Based upon these results, laboratory-scale test samples of different double walls with Helmholtz resonators are constructed and evaluated using sound intensity measurements in order to demonstrate the improved STL over a broad frequency range. The results of the experimental study are presented in Section 4. Finally, Section 5 provides a summary and the conclusions of this investigation.

Accepted Manuscript

2. Analytical model

This section will provide an analytical model to calculate the sound transmission loss of double walls with Helmholtz resonators. First, a simple model for the effective bulk modulus of a confined fluid volume containing Helmholtz resonators will be derived and validated using impedance tube measurements. Then, this model is applied to calculate the resonance frequencies of a double wall containing Helmholtz resonators. Finally, expressions to obtain the transmission loss of a double wall filled with Helmholtz resonators will be given.

In the following derivations, a time dependency of the form $\exp(\mathrm{i}\omega t)$, with $\mathrm{i} = \sqrt{-1}$, the angular frequency $\omega = 2\pi f$, and the time t, is implicitly assumed and therefore omitted.

2.1. Effective bulk modulus of a fluid volume with Helmholtz resonators

The effective bulk modulus K_{eff} is defined here as the pressure amplitude p inside an air volume V resulting from a dynamic volume change ΔV:

$$K_{\mathrm{eff}} = -V\frac{p}{\Delta V}. \tag{2}$$

It should be noted that ΔV is defined positive if it leads to an increase of the original air volume V. In order to obtain an analytical expression for K_{eff} in the case of a fluid volume with embedded Helmholtz resonators, the simplified model as shown in Fig. 1 is used: A piston imposes a dynamic volume change ΔV on a rigidly bounded fluid volume V which encloses a Helmholtz resonator with a resonator volume V_R. Assuming that all dimensions of the fluid volume are much smaller than the acoustic wavelength λ, the pressure amplitude inside the fluid volume p (but outside of the Helmholtz resonator) can be obtained from the bulk modulus K of the fluid inside the volume via

$$K = -(V - V_R)\frac{p}{\Delta V - \Delta V_R}, \tag{3}$$

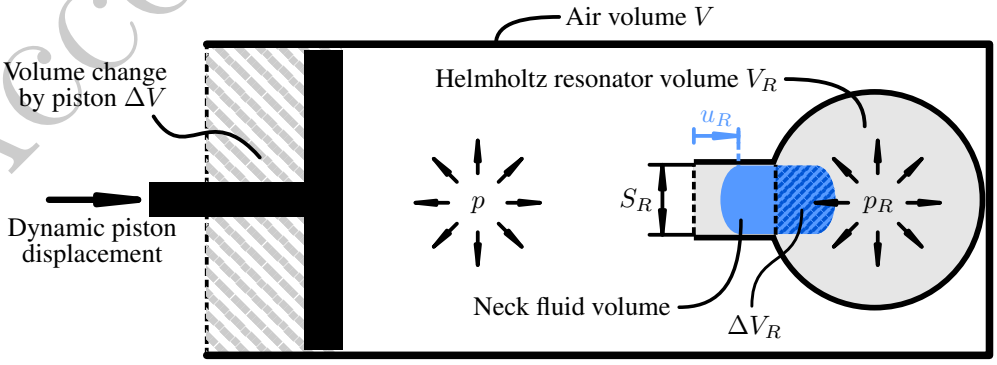

Figure 1: Schematical drawing of the simplified model used to obtain an analytical expression of the effective bulk modulus K_{eff} of a fluid volume with Helmholtz resonators.

Accepted Manuscript

where ΔV_R is the volume change caused by the oscillating fluid inside the neck of the Helmholtz resonator. ΔV_R is defined positive if it leads to an increase of the resonator volume V_R, hence the negative sign inside the denominator of Eq. (3). Combining Eqs. (2) and (3) results in

$$K_{\text{eff}} = \frac{K}{1 - \phi_R - \frac{K}{V}\frac{\Delta V_R}{p}}, \tag{4}$$

where the volumetric filling ratio $\phi_R = V_R/V$ of the resonator has been introduced.

The volume change by the resonator neck ΔV_R is related to the average neck particle displacement u_R and the neck cross-sectional area S_R via $\Delta V_R = -u_R S_R$. The equation of motion of the fluid volume inside the neck is

$$-\omega^2 M_R u_R + \mathrm{i}\omega B_R u_R = (p - p_R)\, S_R, \tag{5}$$

where M_R is the mass of the oscillating neck fluid volume, B_R is the damping coefficient associated with visco-thermal losses at the neck, and p_R is the pressure inside the resonator. Similar to p, the resonator volume pressure p_R is related to the bulk modulus K_R of the fluid inside the resonator through

$$K_R = -V_R \frac{p_R}{\Delta V_R} = V_R \frac{p_R}{u_R S_R}. \tag{6}$$

For generality, the bulk moduli K and K_R can be different, for example when Helmholtz resonators embedded inside a porous matrix are considered. In the common case that both the Helmholtz resonators and the surrounding volume are filled with air, $K = K_R = \rho_0 c_0^2$. Combining Eqs. (5) and (6) and introducing the Helmholtz resonance frequency $\omega_R = \sqrt{K_R S_R^2/(V_R M_R)}$ and damping ratio $\zeta_R = B_R/(2M_R\omega_R)$ results in

$$\frac{M_R}{S_R}(\omega_R^2 + 2\mathrm{i}\zeta_R\omega_R\omega - \omega^2)u_R = p. \tag{7}$$

This can be inserted into Eq. (4) and after some algebraic manipulations the following expression for K_{eff} results:

$$K_{\text{eff}} = \frac{K}{1 - \phi_R + \frac{K}{K_R}\frac{\phi_R}{1 + 2\mathrm{i}\zeta_R\Omega_R - \Omega_R^2}}, \tag{8}$$

with $\Omega_R = \omega/\omega_R$. From Eq. (8) it becomes clear that the effective bulk modulus of a fluid volume with embedded Helmholtz resonator depends only on the bulk modulus K of the background fluid, volumetric filling ratio ϕ_R, the Helmholtz resonance frequency ω_R, the damping ratio ζ_R, and (if the fluid inside the resonator is different from the background fluid) the bulk modulus K_R of the fluid inside the resonator. In the undamped case ($\zeta_R = 0$) and for the same fluid properties inside and outside of the resonator ($K/K_R = 1$), Eq. (8) simplifies to

$$K_{\text{eff}} = K\frac{1 - \Omega_R^2}{1 - (1 - \phi_R)\,\Omega_R^2}. \tag{9}$$

The same modeling approach can be followed if multiple Helmholtz resonators with different properties

Accepted Manuscript

should be considered inside the volume V. In this case, the expression for K_{eff} changes to

$$K_{\text{eff}} = \frac{K}{1 - \phi_R + \sum_{i=1}^{N} \frac{K}{K_{R,i}} \frac{\phi_{R,i}}{1+2\mathrm{i}\zeta_{R,i}\Omega_{R,i}-\Omega_{R,i}^2}}, \tag{10}$$

where i is the index of each Helmholtz resonator in V, N is the number of resonators, and ϕ_R corresponds to the volumetric filling ratio of all resonators together.

The analytical model for the effective bulk modulus of a Helmholtz resonator is verified using impedance tube measurements according to the 4-microphone-method (ASTM E2611-09) [17]. This measurement method allows the experimental determination of the transfer matrix elements T_{11}, T_{12}, T_{21}, and T_{22} of the test specimen. These values can then be used to calculated the effective characteristic impedance $Z_{\text{eff}} = \sqrt{T_{12}/T_{21}}$ and the effective wave number $k_{\text{eff}} = (\cos^{-1} T_{11})/a$, with a being the specimen thickness. With k_{eff} and Z_{eff}, the effective bulk modulus $K_{\text{eff}} = \omega Z_{\text{eff}}/k_{\text{eff}}$ and the effective density $\rho_{\text{eff}} = k_{\text{eff}} Z_{\text{eff}}/\omega$ are calculated. Fig. 2(a) illustrates the general test setup. A Brüel & Kjær type 4206 impedance tube with a diameter of $D = 100$ mm and four flush mounted type 4187 pressure microphones was employed. The measurement frequency range of the impedance tube is specified as $f = 50 \ldots 1600$ Hz. The fluid density and speed of sound during the measurements were determined at $\rho_0 = 1.22\ \mathrm{kg\,m^{-3}}$ and $c_0 = 344\ \mathrm{m\,s^{-1}}$, respectively.

The investigated Helmholtz resonator consists of a spherical cavity with diameter $D_R = 38.3$ mm and a

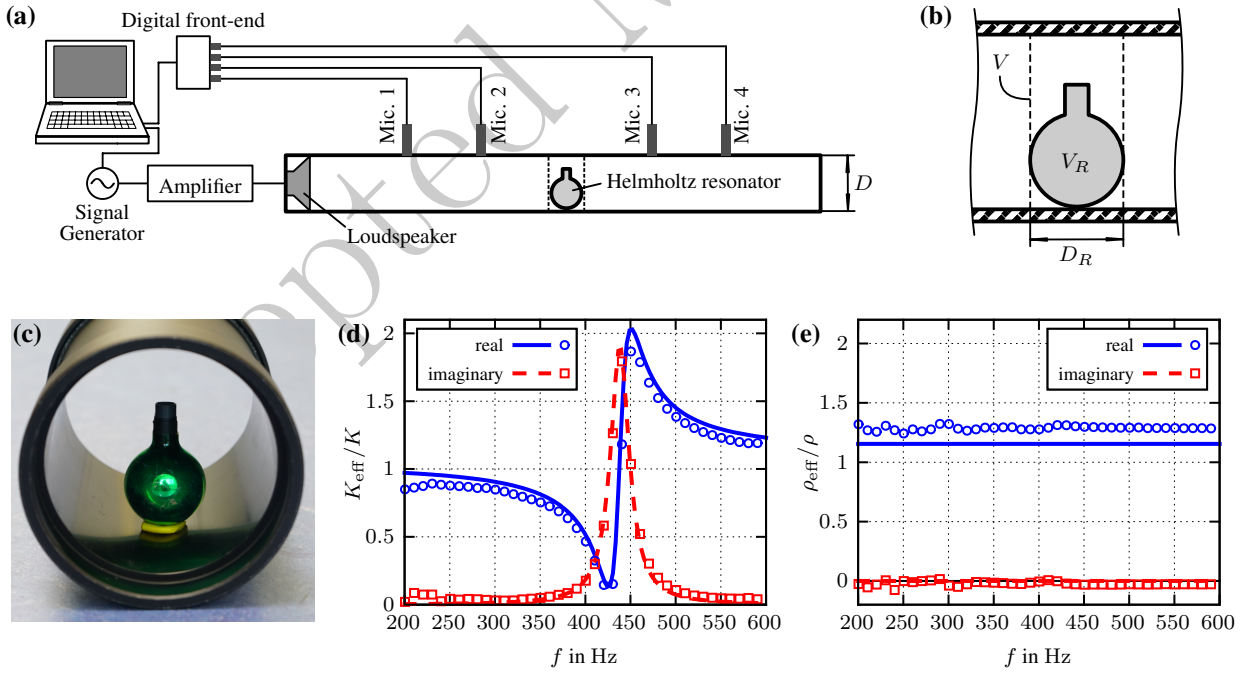

Figure 2: Impedance tube measurement of the effective bulk modulus K_{eff} of a fluid volume with Helmholtz resonator. (a) Schematic overview of the impedance tube measurement setup; (b) Detail of the Helmholtz resonator in the impedance tube and definition of the reference volume V; (c) Photograph of the measured Helmholtz resonator; (d) Comparison of experimental (symbols) and analytical results (curves) for the complex effective bulk modulus; (e) Comparison of experimental (symbols) and analytical results (curves) for the complex effective density.

Accepted Manuscript

neck with a length of $L_R = 21$ mm and circular open cross-section $S_R = 46.6$ mm^2 (radius $R_R = 3.85$ mm). The mass of the fluid volume inside the neck M_R can be estimated as $M_R \approx \rho_0 S_R(L_R + 2 \cdot 0.82 R_R) \approx 1.55$ mg [18]. Thus, for this resonator geometry, the Helmholtz resonance frequency is given by approximately $f_R \approx 417$ Hz. The resonator was mounted vertically inside the sample holder of the impedance tube, as shown in Fig. 2(b), by fixing the bottom of the resonator to the impedance tube wall using putty. Fig. 2(c) shows a photograph of the Helmholtz resonator inside the sample holder. The sample thickness a, which is required to obtain the effective material parameters in the measurements, can be specified somewhat arbitrarily. It should, however, be within some physically reasonable bounds: The sample thickness cannot be smaller than the sample itself and it should be much smaller than the acoustic wavelength λ. In order to obtain the highest possible filling ratio, the resonator diameter D_R was specified as the sample thickness, as illustrated in Fig. 2(b). The reference volume V which is used to obtained the volumetric filling ratio $\phi_R = V_R/V$ for the analytical model is then given by the extrusion of the impedance tube cross-section along the sample thickness, i.e. $V = 0.25\pi D^2 D_R$. From this it follows that the volumetric filling ratio for this test sample is $\phi_R = (\pi D_R^3/6)/(0.25\pi D^2 D_R) = 2/3(D_R/D)^2 \approx 9.8$ %. Finally, the damping ratio ζ_R was estimated from the measurement data as $\zeta_R \approx 3$ %.

The obtained effective bulk modulus of the Helmholtz resonator (normalized by the bulk modulus K of the background fluid) is shown in Fig. 2(d) between $f = 200$ and 600 Hz. The symbols represent the measured data and the lines correspond to analytical results using Eq. (8). The blue circles/solid lines are the real part of K_{eff}, while the red squares/dashed lines are the imaginary part. Overall, a good agreement between the experimental and analytical results can be observed. Some slight differences can be seen particularly for the real part of K_{eff} at low frequencies. This most likely is a consequence of measurement inaccuracies in the 4-microphone-method at low frequencies. For $f \to 0$ Hz, the effective bulk modulus of the Helmholtz resonator corresponds to that of the background fluid ($K_{\text{eff}}/K \approx 1$). For higher frequencies up to the Helmholtz resonance frequency $f_R \approx 417$ Hz, K_{eff} becomes smaller and reaches nearly zero close to f_R. This means that close to the Helmholtz resonance frequency, a fluid volume with Helmholtz resonator becomes very soft compared to the same fluid volume without resonator. Then, the effective bulk modulus increases quickly and the magnitude of K_{eff} reaches its maximum value at around $f_R/\sqrt{1-\phi_R} \approx 439$ Hz (the so-called tonraum resonance frequency [7]). After this frequency, the resonator becomes decoupled from the background fluid volume and the effective bulk modulus asymptotically approaches $K_{\text{eff}} \to K/(1-\phi_R)$, i.e. the fluid volume becomes stiffer. Additionally, Fig. 2(e) shows the measured results for the effective density ρ_{eff} of the fluid volume with Helmholtz resonator, normalized by the ambient air density ρ. The measured effective density is nearly constant over the considered frequency range, but approximately 30 % larger than that of the air. This can be explained by the tortuosity of the impervious Helmholtz resonator which leads to an increase of the apparent mass of the fluid volume containing the resonator [19]. The increased effective density can be

Accepted Manuscript

estimated using the analytical formula by Berryman [20] for spherical inclusions

$$\rho_{\text{eff}} \approx \rho \frac{2+\phi_R}{2\,(1-\phi_R)}, \tag{11}$$

where it is assumed that the density of the resonators is much larger than the air density. The effective density resulting from Eq. (11) is compared to the measurement results in Fig. 2(e). The analytical results slightly underestimate the experimental results. However, given the simplicity of the expression in Eq. (11) this deviation can be acceptable.

The impact of the filling ratio ϕ_R on the effective parameters K_{eff} and ρ_{eff} is illustrated in Fig. 3. The magnitude of the effective bulk modulus is shown in Fig. 3(a). It can be seen that below the Helmholtz resonance frequency f_R an increase of the filling ratio leads to a stronger reduction of the effective stiffness of the fluid volume. On the other hand, at higher frequencies the maximum effective bulk modulus value at the tonraum frequency increases and the tonraum frequency itself is increased, since it is proportional to $1/\sqrt{1-\phi_R}$. After this frequency, the asymptotic value of the effective bulk modulus is larger for higher filling ratios. This can be explained by the larger volume occupied by the Helmholtz resonator essentially constraining the compression of the background fluid. For the effective density shown in Fig. 3(b) it follows that an increase of the filling ratio increases the tortuosity resulting from the resonators which therefore leads to an increase of the resulting effective density.

2.2. Mass-air-mass resonance frequency of a double wall with Helmholtz resonators

The analysis in the previous sub-section shows that the stiffness of a fluid volume can be significantly modified at certain frequencies by inserting Helmholtz resonators into the volume. It is particularly interesting that below the Helmholtz resonance frequency the effective bulk modulus of the fluid volume is smaller than the bulk modulus of the background medium. Since, as evident from Eq. (1), the mass-air-mass resonance frequency of a double wall can be reduced if the bulk modulus is decreased, this sub-section investigates the impact of Helmholtz resonators on the mass-air-mass resonance frequency.

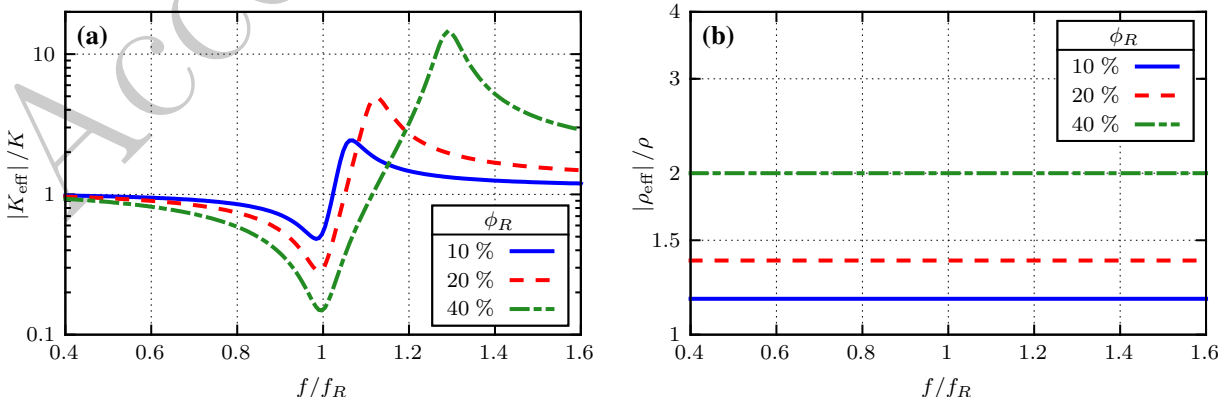

Figure 3: Magnitude of the effective material parameters for different volumetric filling ratios ϕ_R. (a) Effective bulk modulus; (b) Effective density.

Accepted Manuscript

In order to calculate the resonance frequencies of a double wall with Helmholtz resonators inside the air gap, Eq. (9) for the undamped case of the effective bulk modulus of a fluid volume with Helmholtz resonators can be inserted into Eq. (1) with $\omega \to \omega_0 = 2\pi f_0$. This approach is equivalent to representing the double wall as the mechanical oscillator shown in Fig. 4(a), where the walls are modelled as masses m_1'' and m_2'' and the fluid volume with Helmholtz resonator corresponds to a spring with *frequency-dependent* stiffness $K_{\mathrm{eff}}(\omega)/H$. Solving the resulting equation for the resonance frequency f_0 yields after some algebraic manipulations

$$f_0^2 = \frac{1 + \frac{f_R^2}{f_{\mathrm{DW}}^2} \pm \sqrt{\left(1 - \frac{f_R^2}{f_{\mathrm{DW}}^2}\right)^2 + 4\phi_R \frac{f_R^2}{f_{\mathrm{DW}}^2}}}{2\left(1 - \phi_R\right)} f_{\mathrm{DW}}^2, \tag{12}$$

where f_{DW} is the mass-air-mass resonance frequency of the double wall without Helmholtz resonators (but otherwise equal surface mass densities and wall spacing). The result in Eq. (12) shows that the double wall system now exhibits two resonance frequencies which both depend only on f_{DW}, f_R, and ϕ_R.

Fig. 4(b) shows the variation of the two resonance frequencies given in Eq. (12) with the Helmholtz resonance frequency f_R varying between 0 and 2 times f_{DW} for three different volumetric filling ratios $\phi_R = 20\,\%$, $50\,\%$, and $80\,\%$. It can be seen that if $f_R \ll f_{\mathrm{DW}}$, the first resonance frequency f_{01} is nearly independent of the filling ratio and goes to zero as $f_R \to 0$. The second resonance frequency f_{02}, on the other hand, exhibits a strong dependency on ϕ_R and approaches a constant value of $f_{\mathrm{DW}}/\sqrt{1-\phi_R}$ for very small Helmholtz resonance frequencies. As f_R is increased, the first resonance frequency increases as well and converges to f_{DW} for $f_R \gg f_{\mathrm{DW}}$. The volumetric filling ratio determines how quickly the first resonance frequency approaches f_{DW}: The smaller ϕ_R, the closer f_{01} will be to the original mass-air-mass resonance

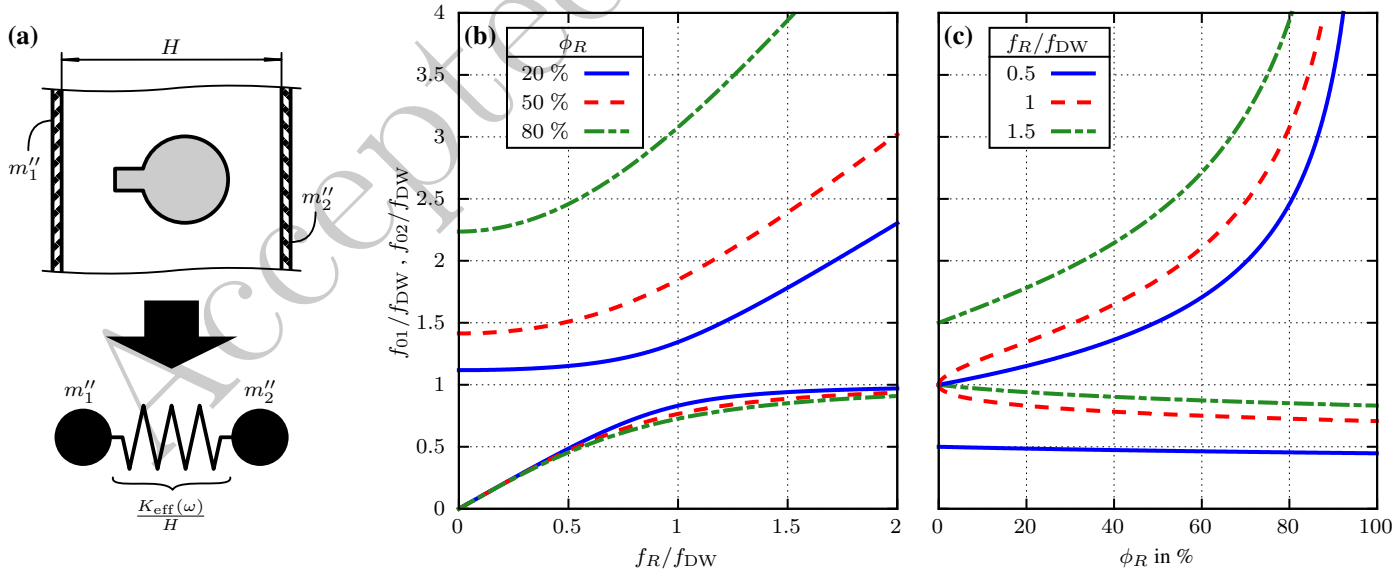

Figure 4: Resonance frequencies f_0 of a double wall with Helmholtz resonators. (a) Mechanical model of the double wall representing the walls by rigid bodies and the fluid volume with Helmholtz resonator by a frequency-dependent effective bulk modulus according to Eq. (9); (b) Variation of the resonance frequencies with the Helmholtz resonance frequency f_R; (c) Variation of the resonance frequencies with the volumetric filling ratio ϕ_R.

Accepted Manuscript

frequency for a given Helmholtz resonance frequency f_R.

In Fig. 4(c) it is shown how the volumetric filling ratio ϕ_R affects the double wall resonance frequencies for the three different values of $f_R/f_{\mathrm{DW}} = 0.5$ (i.e. Helmholtz resonator tuned lower than the original mass-air-mass resonance frequency), 1 (tuned equal to f_{DW}), and 1.5 (tuned higher than f_{DW}). For $\phi_R = 0$ (corresponding to no resonators between the walls), the resonance frequencies are equal to f_R and f_{DW}. This means that the original behavior of the double wall without Helmholtz resonators is retained, because no Helmholtz resonators are present inside the double wall and Eq. (12) yields the solutions of the two decoupled systems: the empty double wall and the Helmholtz resonators (which are not present inside the double wall). When the filling ratio is increased, the first resonance frequency becomes lower, because, for frequencies below f_R, the stiffness of the air volume becomes smaller. In the limit $\phi_R \to 1$, the first resonance frequency goes to $f_{01} \to f_R/\sqrt{1+(f_R/f_{\mathrm{DW}})^2}$. The second resonance frequency, on the other hand, increases with ϕ_R and goes to infinity as the filling ratio approaches 100 %.

The red dashed pair of curves in Fig. 4(c), which correspond to the special case where the Helmholtz resonator is tuned exactly equal to the mass-air-mass resonance frequency, will now be discussed in more detail, because this case has received more attention in the literature [4, 6, 21]: At $\phi_R = 0$ (i.e. no Helmholtz resonators), both curves start at $f_0/f_{\mathrm{DW}} = 1$ which means that, naturally, the mass-air-mass resonance frequency of the double wall is not changed. As the filling ratio of Helmholtz resonators is increased, both resonance frequency curves separate from each other, with one resonance frequency slowly decreasing while the other frequency quickly increases. The first resonance frequency can be interpreted as the new mass-air-mass resonance frequency of the double wall with embedded Helmholtz resonators. It is obvious from Fig. 4(c) that the mass-air-mass resonance frequency can be reduced by introducing Helmholtz resonators. However, the reduction cannot be arbitrarily large: For $f_R/f_{\mathrm{DW}} = 1$, the lowest possible value of the mass-air-mass resonance frequency at $\phi_R = 1$ is $f_{\mathrm{DW}}/\sqrt{2}$, that is approximately 70 % of the mass-air-mass resonance frequency of the unmodified double wall. According to Eq. (1), this effectively corresponds to a doubling of the wall spacing H or the wall masses m_1'' and m_2''. If the Helmholtz resonator is tuned to frequencies greater than f_{DW}, the maximum possible mass-air-mass resonance frequency reduction is smaller. For example, if $f_R = 2f_{\mathrm{DW}}$, then the lowest possible value of the new mass-air-mass resonance frequency will be approximately 90 % of the value of f_{DW}.

In the case that the Helmholtz resonance frequency is smaller than f_{DW}, the change of the mass-air-mass resonance frequency is different: It can be seen in Fig. 4(c) for $f_R/f_{\mathrm{DW}} = 0.5$ that the original mass-air-mass resonance frequency increases as the filling ratio is increased. This is because for frequencies $f \gg f_R$ the effective bulk modulus of a fluid volume with Helmholtz resonators becomes greater than the bulk modulus of the background fluid. However, in the following sub-section it will be shown that this can also lead to a significant improvement of the STL of the double wall.

2.3. Sound transmission loss of a double wall with Helmholtz resonators

Mason and Fahy [4] already provided an analytical model for calculating the sound transmission loss of

Accepted Manuscript

double walls with Helmholtz resonators. In their derivation, the authors do not consider the volume of the Helmholtz resonators a part of the air cavity between the walls. For significant filling ratios (e.g. $\phi_R \gtrsim 5\,\%$), however, the volume occupied by the resonators can be very important. Furthermore, the transmission of obliquely incident sound waves or diffuse sound fields was not considered in Ref. [4]. Therefore, this contribution provides an improved method for predicting the sound transmission properties of double walls with Helmholtz resonators which is applicable even when the filling ratio of the resonators is quite large and oblique or diffuse incident sound fields are to be considered.

As shown in Sub-section 2.1, the fluid volume with Helmholtz resonators between the two walls can be represented by an equivalent fluid with effective bulk modulus and density given by Eqs. (8) and (11), respectively. Therefore, an analytical expression for the transmission coefficient τ can be obtained by considering the transmission of plane acoustic waves through a double wall at an incidence angle of θ_0 with different fluid properties inside and outside the double wall. Following the same steps as for a normal double wall (see, for example, Ref. [1, pp. 314–316]), but taking into account the effective impedance $Z_\mathrm{eff} = \sqrt{K_\mathrm{eff}\rho_\mathrm{eff}}$, effective wave number $k_\mathrm{eff} = \omega\sqrt{\rho_\mathrm{eff}/K_\mathrm{eff}}$, and angle of refraction θ_eff (which is related to θ_0 via Snell's law: $\sin\theta_\mathrm{eff} = \sin\theta_0\sqrt{K_\mathrm{eff}/\rho_\mathrm{eff}}/c_0$), the following expression for the transmission coefficient can be obtained:

$$\tau = \left| \frac{2\mathcal{Z}\sin(k_\mathrm{eff} H\cos\theta_\mathrm{eff})}{\mathcal{X}_1\mathcal{X}_2\sin^2(k_\mathrm{eff} H\cos\theta_\mathrm{eff}) + \mathcal{Z}^2} \right|^2 , \tag{13}$$

where $\mathcal{Z} = Z_\mathrm{eff}\sec\theta_\mathrm{eff}/(Z_0\sec\theta_0)$, $\mathcal{X}_{1/2} = X_{1/2}\cos\theta_0 + 1 - \mathrm{i}\mathcal{Z}\cot(k_\mathrm{eff} H\cos\theta_\mathrm{eff})$, and $X_{1/2} = \mathrm{i}\omega m''_{1/2}/Z_0$ are the normalized wall impedances of the two walls. The sound transmission loss is then given by $\mathrm{TL} = -10\lg\tau$. For normal incidence and frequencies with sound wavelengths much larger than the wall spacing H, Eq. (13) can be simplified to

$$\tau = \left| \frac{2\mathcal{K}}{(X_1 + 1 + \mathcal{K})\,(X_2 + 1 + \mathcal{K}) - \mathcal{K}^2} \right|^2 , \tag{14}$$

with $\mathcal{K} = K_\mathrm{eff}/(\mathrm{i}\omega H Z_0)$.

Fig. 5 shows the calculated normal incidence transmission loss results for a double wall ($m''_1 = m''_2 = 1\,\mathrm{kg\,m^{-2}}$, $H = 50\,\mathrm{mm}$, $f_\mathrm{DW} = 380\,\mathrm{Hz}$) with Helmholtz resonators (baseline parameters $\phi_R = 50\,\%$, $f_R/f_\mathrm{DW} = 1.5$, $\zeta_R = 5\,\%$). In the bottom row of plots in Fig. 5, the insertion loss $\Delta\mathrm{TL}$ is shown which is defined as the transmission loss difference between the double wall with and without Helmholtz resonators. The arrows in the plots indicate the resonance frequencies of the double wall calculated using Eq. (12).

The first column in Fig. 5 displays the results for fixed Helmholtz resonance frequency and varying filling ratio. The calculated resonance frequencies correspond well to the STL minima of the double wall. While the lower resonance frequency (the original mass-air-mass resonance frequency) is slightly reduced with increasing filling ratio, the second resonance frequency quickly grows from nearly 700 Hz to over 1.5 kHz. This was already discussed with respect to the results in Fig. 4(c). This spreading of the resonance frequencies as well as the strong STL improvement at the Helmholtz resonance frequency (in this case 570 Hz) leads to the emergence of a very broadband improvement of the transmission loss of the double wall. The insertion loss

Accepted Manuscript

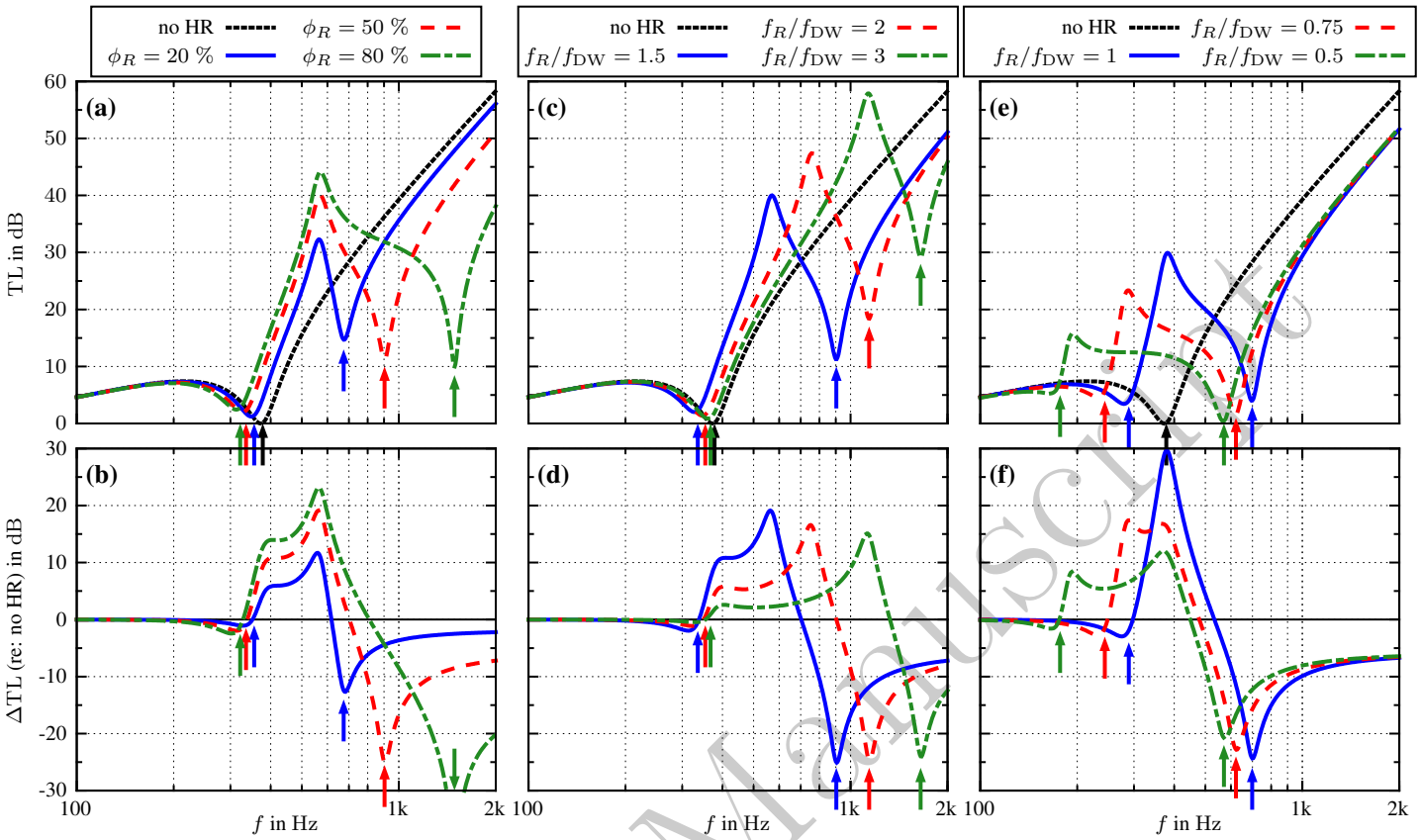

Figure 5: Normal incidence sound transmission loss TL and insertion loss ΔTL (with respect to the case without Helmholtz resonators) of a double wall with Helmholtz resonators. Arrows indicate the resonance frequencies of the double wall obtained from Eq. (12). (a) and (b) Transmission loss and insertion loss for different filling ratios; (c) and (d) Transmission loss and insertion loss for different Helmholtz resonance frequencies $f_R > f_{DW}$; (e) and (f) Transmission loss and insertion loss for different Helmholtz resonance frequencies $f_R \leq f_{DW}$.

shown in Fig. 5(b) makes this particularly clear: A plateau of significant STL improvement appears between the lowest resonance frequency of the double wall with Helmholtz resonators and the Helmholtz resonance frequency. For $\phi_R = 20$ %, the ΔTL is at least 6 dB over a frequency range of 160 Hz. At 50 % filling ratio there is an improvement by more than 10 dB over an even broader frequency range of 240 Hz. This is further increased at $\phi_R = 80$ %, where ΔTL values over 12 dB can be achieved over 275 Hz. Thus, it can be seen that broadband STL improvement can be achieved by using Helmholtz resonators inside a double wall. It should be emphasized that these results do not even take into account any added mass from the resonators which would further improve the STL of the double wall.

Fig. 5(c) and (d) show the transmission and insertion loss for fixed filling ratio and varying Helmholtz resonance frequency f_R. In these calculations, the Helmholtz resonators have been tuned at frequencies higher than the mass-air-mass resonance frequency of the unmodified double wall. Again, a considerable improvement of the double wall STL over a relatively wide frequency range can be observed. As in the results for the filling ratio variation, this is a consequence of the resonance frequency spreading when Helmholtz resonators are introduced. Fig. 5(d) shows that increasing the Helmholtz resonance frequency f_R leads

Accepted Manuscript

to a broadening of the ΔTL-plateau. However, since also the mass-air-mass resonance frequency increases with f_R and asymptotically reaches the mass-air-mass resonance frequency of the unmodified double wall (see Fig. 4(b)), the STL improvement at the plateau will be reduced: At $f_R/f_{\mathrm{DW}} = 2$ there is over 5 dB improvement for 470 Hz, while in the case of $f_R/f_{\mathrm{DW}} = 3$ a much larger plateau width (915 Hz) but with only $\Delta\mathrm{TL} \geq 2$ dB can be achieved.

Similar effects can be observed when the Helmholtz resonance frequency is tuned equal or below the mass-air-mass resonance frequency of the unmodified double wall (see Fig. 5(e) and (f)). For $f_R = f_{\mathrm{DW}}$, one very large STL peak with ΔTL values of nearly 30 dB appears. When the Helmholtz resonance frequency is reduced, the single peak in the insertion loss in Fig. 5(f) splits up into two peaks with the first peak corresponding to f_R and the second peak at f_{DW}. As a result, a ΔTL-plateau forms between these two peaks. Like in the other case with $f_R > f_{\mathrm{DW}}$, the height of the plateau becomes smaller as f_R is shifted further away from the mass-air-mass resonance frequency of the unmodified double wall.

So far, the discussion of the results shown in Fig. 5 has focused on the STL improvement due to the Helmholtz resonators and how this improvement is affected by ϕ_R and f_R. It should be emphasized, however, that this improvement comes along with a decrease in sound insulation performance of the double wall at higher frequencies. The decrease of the STL is the largest at the second resonance frequency f_{02} and then the insertion loss approaches a constant value of approximately $\Delta\mathrm{TL} \approx 20\lg(1-\phi_R) < 0$. This high frequency STL decrease is caused by the decoupling of the resonator fluid volume from the rest of the double wall cavity which occurs at frequencies above f_R. Thus, the wall spacing of the double wall H is effectively reduced at higher frequencies, leading to the reduced STL compared to the double wall without resonators.

To get a better impression of the high frequency effect of the Helmholtz resonators, Fig. 6 shows the transmission loss and insertion loss of a double wall ($m_1'' = m_2'' = 1\ \mathrm{kg\,m^{-2}}$, $H = 50$ mm, $f_{\mathrm{DW}} = 380$ Hz) with Helmholtz resonators ($\phi_R = 50\ \%$, $f_R/f_{\mathrm{DW}} = 1.5$, $\zeta_R = 5\ \%$) for up to $f = 5$ kHz. The results have

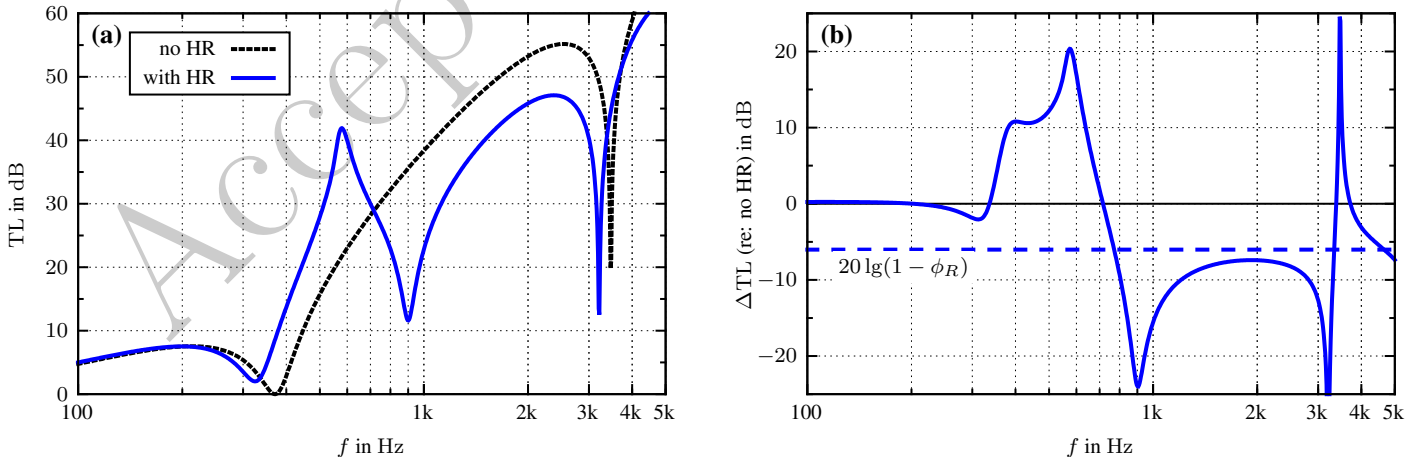

Figure 6: Normal incidence sound transmission loss TL and insertion loss ΔTL (with respect to the case without Helmholtz resonators) of a double wall with Helmholtz resonators for an extended frequency range up to 5 kHz. (a) Transmission loss TL; (b) Insertion loss ΔTL.

Accepted Manuscript

been calculated using Eq. (13). It should be noted that the homogenization approach to obtain K_{eff} and ρ_{eff} of the fluid volume with Helmholtz resonators is valid as long as the height of the fluid volume is smaller than the wavelength. Thus, a maximum frequency of 5 kHz has been chosen to ensure that $H < \lambda$. Fig. 6(a) shows that above approximately 700 Hz the STL of the double wall with Helmholtz resonators is below the transmission loss of the corresponding double wall without resonators over a wide range of frequencies. The insertion loss shown in Fig. 6(b) clearly approaches the dashed line at $20\lg(1-\phi_R) \approx -6$ dB at around 2 kHz. In this frequency range the Helmholtz resonators are decoupled and the volume of the double wall cavity is effectively reduced by half. Between 3 and 4 kHz it can be also seen that the first $\lambda/2$-resonances occur for both double wall configurations. For the double wall without Helmholtz resonators, this resonance occurs at the frequency $c_0/(2H) \approx 3.4$ kHz. When the resonators are introduced, this resonance frequency is slightly reduced. The reason for this is that the effective speed of sound of the fluid volume is given by $c_{\text{eff}} = \sqrt{K_{\text{eff}}/\rho_{\text{eff}}}$ and for frequencies $f \gg f_R$ it follows from Eqs. (9) and (11) that c_{eff} will be smaller than c_0 and approaches $c_{\text{eff}}/c_0 \approx \sqrt{2/(2+\phi_R)}$. Thus, for the configuration shown in Fig. 6 the $\lambda/2$-resonance is reduced to 3.04 kHz with included Helmholtz resonators.

In summary, the presented results for the sound transmission loss of a double wall with Helmholtz resonators reveal that it is possible to achieve broadband STL improvement at low frequencies compared to a double wall without Helmholtz resonators. This approach is different from previous investigations of Helmholtz resonator double walls, where the primary target was to achieve STL improvements specifically at the Helmholtz resonance frequency. At high frequencies, however, it has to be accepted that the transmission loss of the double wall will be decreased due to the Helmholtz resonators. Thus, there is a certain trade-off between an improved low-frequency STL over a broad frequency range and a decreased sound insulation at high frequencies. The extent of this trade-off depends on the target noise control problem: If the noise source is dominated by low-frequency noise (for example a propeller-driven aircraft with changing rotational speeds of the propellers), then an impact at higher frequencies can be accepted for the sake of improving the critical low-frequency range. Also, at high frequencies most practical double wall constructions are dominated by the structure-borne sound path along the structural connections between the walls [1], which is not considered here. Thus, it can be expected that the air-borne path with the Helmholtz resonators will be negligible compared to the structure-borne path above a certain frequency and the STL values of the double walls with and without resonators will become similar. Finally, the reduced STL at higher frequencies could also be alleviated by introducing porous absorbers (such as glass wool or open-celled foams) which are more efficient at absorbing sound at higher frequencies.

3. Parameter studies

The STL calculation results in Fig. 5 indicate that a ΔTL plateau occurs roughly between the unmodified mass-air-mass resonance frequency f_{DW} and the Helmholtz resonance frequency f_R. The purpose of the parameter studies in this section is to investigate how the properties of this plateau are affected by the

Accepted Manuscript

different design parameters of a double wall with Helmholtz resonators. First, it is shown how the insertion loss plateau can be optimized to achieve broadband sound insulation by selecting suitable parameters for the Helmholtz resonators and the resulting high-frequency behavior is discussed. Then, Sub-section 3.2 explores how the plateau is affected by the parameters of the double wall. All calculations in this section have been performed for normal incidence using Eq. (14).

3.1. Insertion loss plateau optimization

The plateau can be characterized by the relative bandwidth $B = (f_u - f_l)/\sqrt{f_l f_u}$, where f_l and f_u are the lower and upper limiting frequencies of the frequency band around f_R for which $\Delta\mathrm{TL} > 0$. Since the height of the plateau is also affected by the Helmholtz resonators, the average $\Delta\mathrm{TL}$ of the plateau, which is defined as

$$\overline{\Delta\mathrm{TL}} = \frac{1}{f_u - f_l} \int_{f_l}^{f_u} \Delta\mathrm{TL}\,\mathrm{d}f, \tag{15}$$

will be used to characterize the magnitude of the STL improvement.

In Fig. 7(a) it is shown how the bandwidth of the STL improvement plateau is affected by the resonator filling ratio ϕ_R and the Helmholtz resonance frequency f_R (normalized by f_{DW}). In general, it becomes clear that higher bandwidths can be achieved by increasing the volumetric filling ratio of the resonators. The results in Fig. 7(a) are quite symmetric with respect to the horizontal line at $f_R/f_{\mathrm{DW}} = 1$. This indicates that similar bandwidths can be achieved by tuning the resonators to either higher or to lower frequencies than the mass-air-mass resonance frequency of the double wall by the same factor (e.g. twice or half the value of f_{DW}). The lowest bandwidth values (for constant ϕ_R) occur when the resonators are tuned exactly to f_{DW}. As f_R/f_{DW} becomes larger or lower than unity, the bandwidth increases significantly. This is in line with the results shown in Fig. 5(d) and (e) where it was observed that a larger gap between f_R and f_{DW} leads to a higher spread between the resonance frequencies of the double wall with Helmholtz resonators. This directly results in the broadening of the insertion loss plateau.

Fig. 7(b) shows the effect of the same Helmholtz resonator parameters on the average $\Delta\mathrm{TL}$ of the plateau. Again, the results exhibit a symmetry about $f_R/f_{\mathrm{DW}} = 1$ and the $\overline{\Delta\mathrm{TL}}$ values are larger for higher filling ratios ϕ_R. However, contrary to the bandwidth in Fig. 7(a), the largest average STL improvement occurs when the Helmholtz resonance frequency and the mass-air-mass resonance frequency are equal. When f_R is higher or smaller than f_{DW} (for example in order to improve the bandwidth), the resulting $\overline{\Delta\mathrm{TL}}$ will be deteriorated.

This contrary behavior of optimizing B and $\overline{\Delta\mathrm{TL}}$ is further illustrated in Fig. 7(c) where both quantities are shown for three different filling ratios and varying f_R/f_{DW}. The arrows indicate the direction in which the parameter f_R/f_{DW} increases along the curves. The peaks of the curves correspond to the point $f_R/f_{\mathrm{DW}} = 1$, which is indicated in Fig. 7(c) by the circles. It can be clearly seen that the bandwidth and height of the insertion loss plateau form a pareto-like front with respect to f_R/f_{DW}: An improvement of the bandwidth

Accepted Manuscript

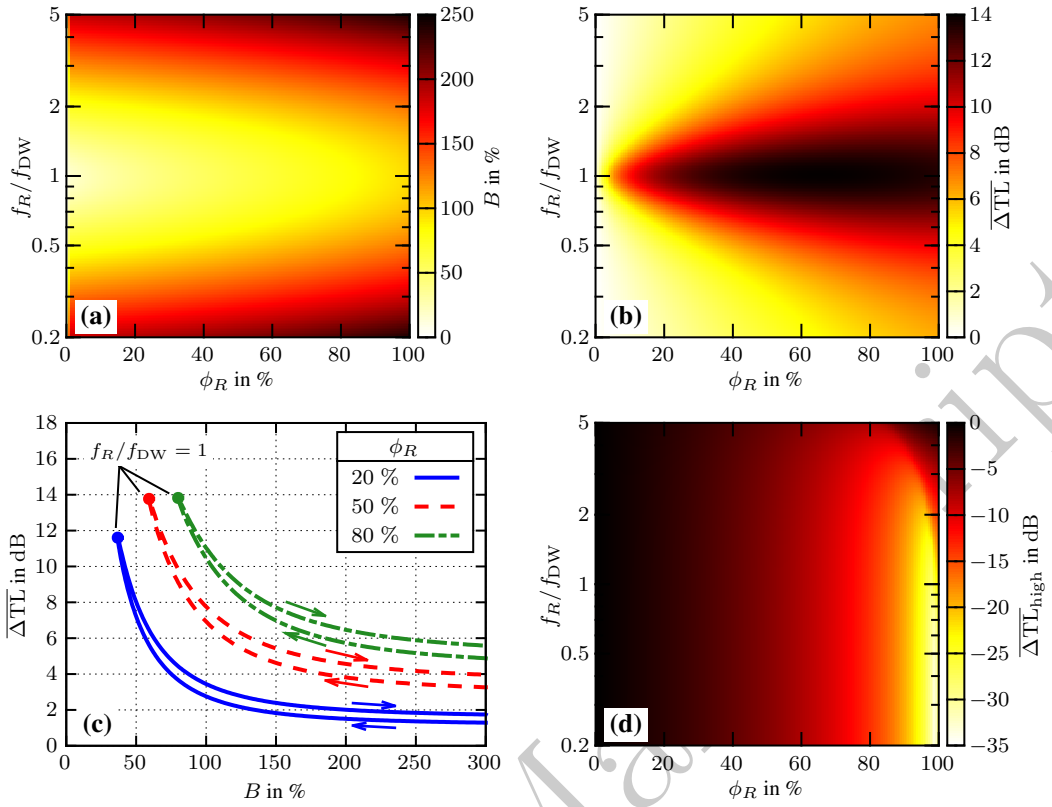

Figure 7: Parametric study of the width and height of the insertion loss plateau. (a) Bandwidth B; (b) Average insertion loss $\overline{\Delta TL}$; (c) Bandwidth and average insertion loss for different filling ratios ϕ_R and varying Helmholtz resonance frequency (the arrows indicate the direction in which f_R/f_{DW} increases and the circles correspond to the points for which $f_R/f_{DW} = 1$); (d) High-frequency average insertion loss $\overline{\Delta TL}_{high}$ from 0 to 5 kHz.

cannot be achieved by changing the Helmholtz resonance frequency without deteriorating the average ΔTL, and vice versa. The filling ratio, on the other hand, can be used to improve both values simultaneously. Therefore, in order to design a Helmholtz resonator double wall with desired broadband improved STL, it is recommended that first the filling ratio should be selected as large as possible. Then, the Helmholtz resonance frequency f_R can be used to fine-tune the properties of the insertion loss plateau. It should be also noted that the shape of the curves in Fig. 7(c) indicates that the results are not perfectly symmetric: If $f_R > f_{DW}$, the width and average height of the plateau will be greater than when the Helmholtz resonance frequency is smaller than f_{DW}.

At the end of Section 2 it was discussed how the transmission loss of a double wall is reduced at high frequencies due to the Helmholtz resonators. This is not problematic in cases where most of the acoustic energy of a noise source is concentrated inside the insertion loss plateau caused by the Helmholtz resonators or when the high-frequency noise components are reduced by other means (e.g. porous absorbers). In some applications, however, it is more appropriate to take into account a larger frequency range than just the insertion loss plateau. For this purpose, Fig. 7(d) shows the variation of the high-frequency average insertion loss $\overline{\Delta TL}_{high}$, which is defined similarly to Eq. (15), but with the integration limits $f_u = 0$ Hz and $f_l = 5$ kHz.

Accepted Manuscript

It can be seen that, in general, $\overline{\Delta \mathrm{TL}}_{\mathrm{high}}$ will always be equal or less than zero when Helmholtz resonators are added to a double wall. This was shown exemplarily in Fig. 6 and cannot be avoided due to the decoupling of the Helmholtz resonator volume for frequencies much higher than f_R. However, it can be seen in Fig. 7(d) that certain resonator configurations have a higher impact on the high-frequency behavior than others: For example, it is in general better for $\overline{\Delta \mathrm{TL}}_{\mathrm{high}}$ to have a low filling ratio while the resonance frequency ratio f_R/f_{DW} has nearly no effect. Only when ϕ_R is very high it can be seen that a large f_R/f_{DW} leads to a smaller STL reduction at high frequencies than when f_R/f_{DW} is small. From the results shown in Fig. 5(d) this becomes clear, since a large Helmholtz resonance frequency stretches out the insertion loss plateau and shifts the STL decrease to even higher frequencies. However, from Fig. 7(b) it is also clear that a large f_R/f_{DW} reduces the STL improvement within the insertion loss plateau. These findings underline the compromise that has to be made regarding the STL improvement at the insertion loss plateau and the overall behavior of the double wall up to high frequencies, when Helmholtz resonators are integrated inside a double wall.

3.2. Effect of the double wall parameters

In order to survey how the parameters of the double wall affect the insertion loss plateau generated by the Helmholtz resonators, further calculations have been performed with a variation of the double wall spacing H and fixed Helmholtz resonator parameters ($f_R/f_{\mathrm{DW}} = 1.5$, $\phi_R = 50\ \%$, $\zeta_R = 5\ \%$). To keep the mass-air-mass resonance frequency of the empty double wall in all cases at $f_{\mathrm{DW}} = 380$ Hz, the wall surface mass densities $m_1'' = m_2''$ have been adjusted accordingly.

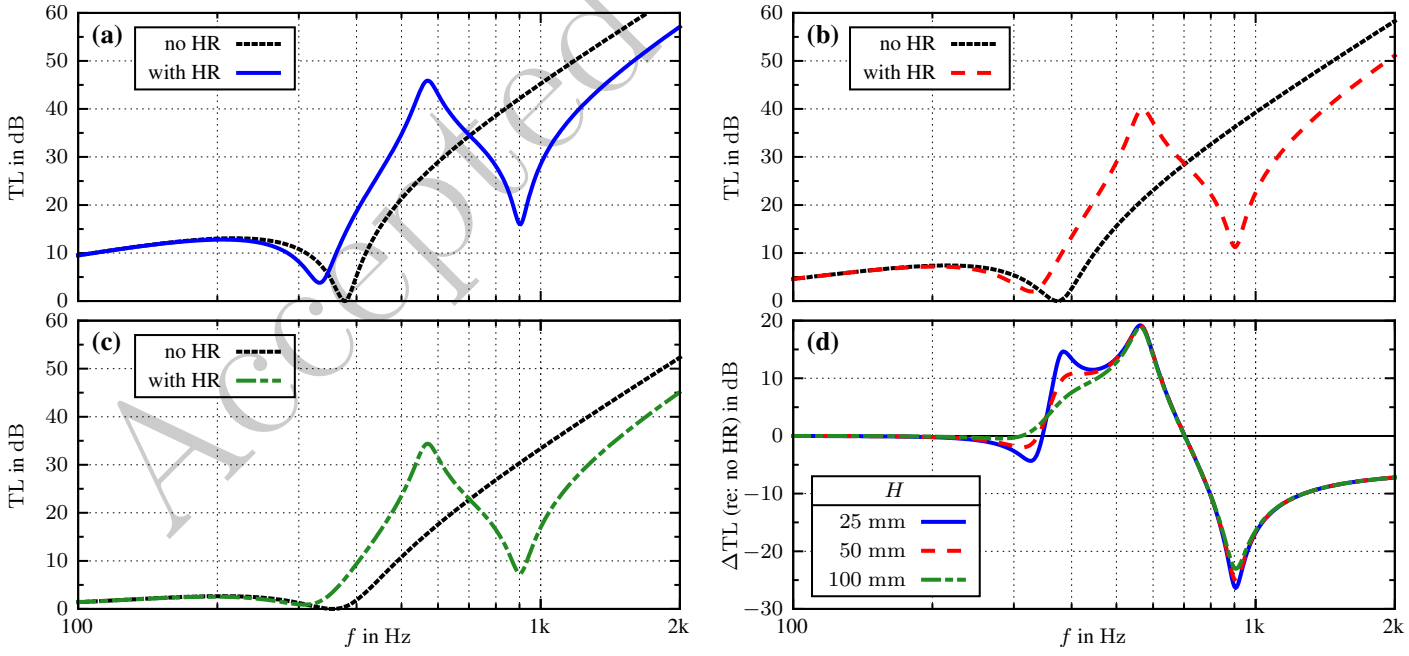

Figure 8: Normal incidence sound transmission loss TL and insertion loss ΔTL (with respect to the case without Helmholtz resonators) of double walls with different wall spacings H and fixed Helmholtz resonator parameters ($f_R = 1.5 f_{\mathrm{DW}}$, $\phi_R = 50\ \%$, $\zeta_R = 5\ \%$). The wall masses $m_1'' = m_2''$ are adjusted to achieve the same mass-air-mass resonance frequency $f_{\mathrm{DW}} = 380$ Hz. (a) $H = 25$ mm; (b) $H = 50$ mm; (c) $H = 100$ mm; (d) Insertion loss ΔTL.

Accepted Manuscript

Fig. 8(a), (b), and (c) show the normal incidence sound transmission loss TL for three different wall spacings $H = 25\,\mathrm{mm}$, $50\,\mathrm{mm}$, and $100\,\mathrm{mm}$, respectively. The corresponding wall masses are given by $m_1'' = m_2'' = 2\,\mathrm{kg\,m^{-2}}$, $1\,\mathrm{kg\,m^{-2}}$, and $0.5\,\mathrm{kg\,m^{-2}}$, respectively. The black dotted curves in Fig. 8(a)–(c) represent the transmission loss of the double walls without Helmholtz resonators. The qualitative shape of the curves in Fig. 8(a)–(c) is similar in all three cases which indicates that the performance of the Helmholtz resonators is at most lightly affected by the parameters of the double wall. In general, a shifting of the curves to higher TL values is observed when the wall spacing is reduced and the wall masses are increased. Since this shifting is also present in the curves for the double walls without Helmholtz resonators, it is a direct consequence of the increased wall masses and cannot be attributed to the Helmholtz resonators.

The small impact of the double wall parameters becomes more clearly visible in Fig. 8(d) where the insertion loss curves are shown for the three different wall spacings. The curves are mostly identical, significant differences are present only around the mass-air-mass resonance frequency and at the second resonance frequency of the double walls with Helmholtz resonators. When the wall spacing is increased, the first dip and peak of the insertion loss plateau are smeared out, leading to a slightly larger bandwidth but also reduced average ΔTL. This effect can be explained by the enhanced fluid damping for higher values of H with smaller wall masses which means that the walls are more easily affected by the surrounding fluid. The fluid damping tends to lower the TL reduction at the resonance frequencies of the double walls and therefore flattens the shape of the insertion loss plateau around f_{DW}. The peak at the Helmholtz resonance $f_R = 570\,\mathrm{Hz}$, on the other hand, is not affected by the fluid damping and therefore is the same in all three cases.

In summary, it can be concluded that the insertion loss plateau is only slightly affected by the double wall parameters. Only for very light double walls the fluid damping leads to a little broadening but also reduction of the insertion loss plateau.

4. Experiment

This section describes experiments that were conducted to validate the analytical model and investigate the broadband improvement of double walls with Helmholtz resonators under diffuse field excitation. In the first sub-section, the test specimens are described, followed by the description of the experimental setup. In the second sub-section, the measurement results are discussed.

4.1. Experimental setup

A Helmholtz resonator panel was designed and manufactured to conduct laboratory scale transmission tests. The test panel has a size of 1 m by 1.2 m and consists of an array of 252 Helmholtz resonators. The panel is made of a lightweight closed-cell polymethacrylimide foam (tradename Rohacell 31 HF). The resonator cavities as well as the necks were milled into the foam, as depicted in Fig. 9(a). The build-up of a unit cell is shown in Fig. 9(b) and (c). The dimensions are listed in Table 1. The resulting volume of each resonator is $V_R = 1.15 \times 10^5\,\mathrm{mm^3}$ and the neck cross-section area accounts for $S_R = 78.5\,\mathrm{mm^2}$. Thus,

Accepted Manuscript

using the approximated air mass inside the resonator neck $M_R \approx \rho_0 S_R(L_R + 2 \cdot 0.82 R_R) \approx 1.72\,\mathrm{mg}$, the resonance frequency is estimated to be $f_R \approx 333\,\mathrm{Hz}$. The back plate of the resonators is formed by a glass fiber reinforced plastic (GFRP) plate with a thickness of 1 mm and a surface mass density of $2\,\mathrm{kg\,m^{-2}}$. The complete panel with the incorporated Helmholtz resonators has a thickness of $H_R = 35\,\mathrm{mm}$ and an overall surface mass density of $m_1'' = 2.9\,\mathrm{kg\,m^{-2}}$.

The setup of a double wall test specimen with the described Helmholtz resonator panel is shown in Fig. 10(a). In this configuration a second wall with surface mass density m_2'' is mounted with a spacing $H = 45\,\mathrm{mm}$ apart from the GFRP back plate with the Helmholtz resonators inside the cavity. The resulting filling ratio is given by $\phi_R = V_R/(l_x l_y H) = 56\,\%$. Fig. 10(b) shows the corresponding reference configuration of an empty double wall, where all Helmholtz resonator were made acoustically inactive by closing their necks with a tape. To maintain the same wall spacing for this mass equivalent reference, wall 2 was shifted apart to reobtain the preselected wall spacing $H = 45\,\mathrm{mm}$, now being measured between wall 2 and the closed Helmholtz resonator surface. This reference is used as a control sample to identify the effect of the Helmholtz resonators in the double wall configurations with active resonators.

Three different double wall designs with Helmholtz resonators were measured to show the influence of the ratio between the Helmholtz resonance frequency and the mass-air-mass resonance frequency (f_R/f_{DW}). The ratio was varied by increasing the surface mass density of the second wall m_2'', while the first wall, i.e. the Helmholtz resonator panel, remained unchanged. The distance between the walls H and accordingly the filling ratio ϕ_R were kept constant. The mass-air-mass resonance frequency f_{DW} decreases with increasing surface mass density of the second wall m_2'', while keeping all the other double wall parameters constant. The parameters of the double wall designs as well as the calculated resonance frequencies are listed in Table 2.

The test samples were mounted in a stiff wooden frame into a test window between a reverberation room and a hemi-anechoic chamber. In the reverberation room, a diffuse sound field was excited by a dodecahedron-loudspeaker with a total sound pressure level of 120 dB, which was measured by a 1/2 inch diffuse field microphone on a rotating beam. In the receiving room, the sound intensity spectrum was

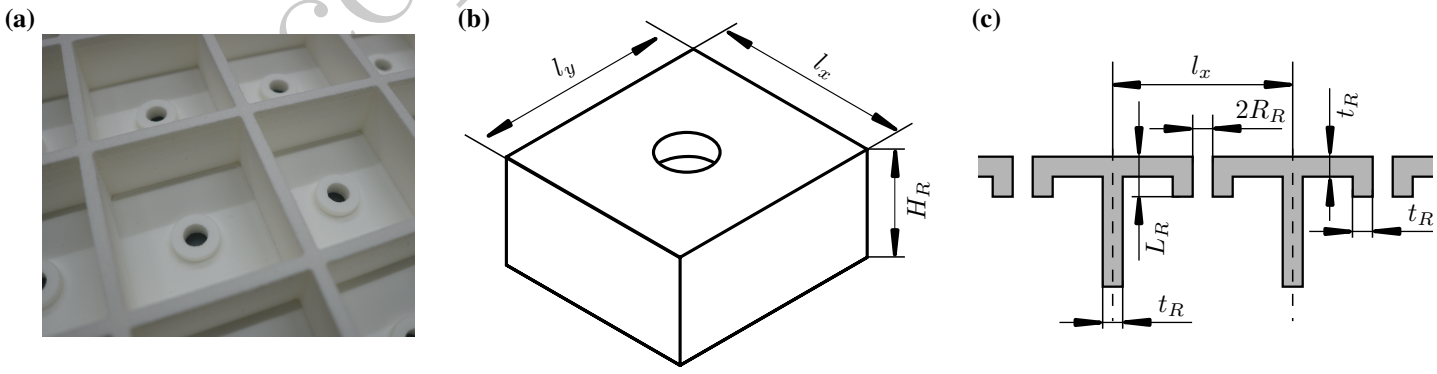

Figure 9: Design of the Helmholtz resonator panel used in the experiments. (a) Photograph of the backside of the resonator panel; (b) Schematic drawing of one unit cell of the Helmholtz resonator; (c) Cropped cross-section of the Helmholtz resonator array shown in (a).

Accepted Manuscript

Table 1: Resonator dimensions of the Helmholtz resonator panel shown in Fig. 9.

Resonator length	l_x	65	mm
Resonator width	l_y	70	mm
Resonator height	H_R	35	mm
Neck radius	R_R	5	mm
Neck length	L_R	10	mm
Wall thickness	t_R	5	mm

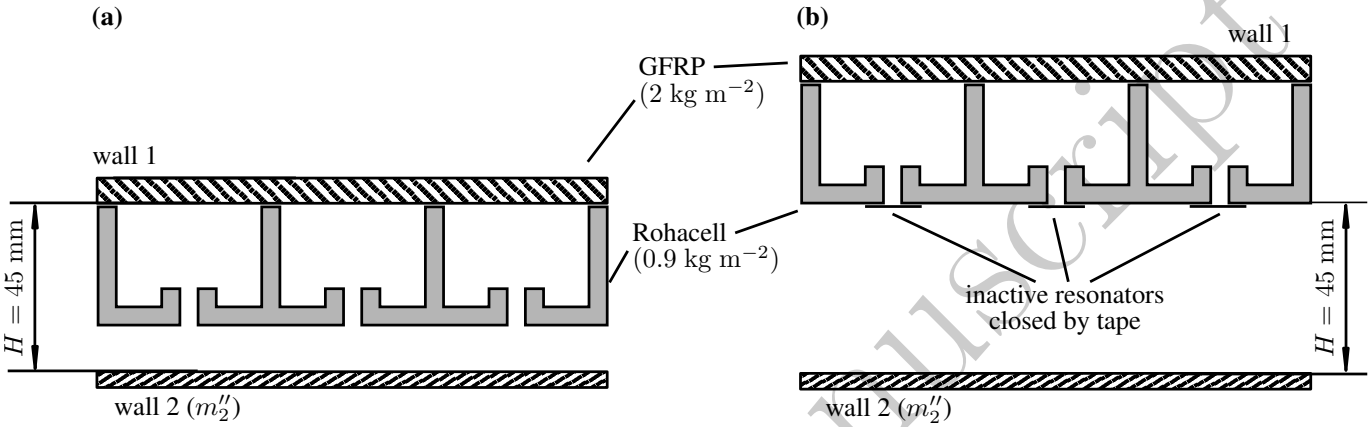

Figure 10: Structure of the double wall test samples. (a) Double wall with active Helmholtz resonators; (b) Double wall with inactive Helmholtz resonators (reference).

measured in 12th-octave bands with a hand-held intensity probe.

The diffuse field transmission coefficient τ_{diff} is obtained from the analytical model by integrating Eq. (13) over the incidence angle θ_0 as follows:

$$\tau_{\text{diff}} = \frac{\int_0^{\theta_{\text{lim}}} \tau(\theta_0) \sin(\theta_0) \cos(\theta_0)\, \mathrm{d}\theta_0}{\int_0^{\theta_{\text{lim}}} \sin(\theta_0) \cos(\theta_0)\, \mathrm{d}\theta_0}, \tag{16}$$

where θ_{lim} is the limiting angle to which the integration is conducted in order to account for the smaller presence of grazing incidence waves in laboratory representations of diffuse sound fields. It should be noted that the investigated double wall test samples did not contain any sound absorbing material within the air

Table 2: Measured designs of the double wall with Helmholtz resonators. The mass-air-mass resonance frequencies f_{DW} and Helmholtz resonator double wall resonance frequencies f_{01} and f_{02} have been calculated for normal incidence using Eqs. (1) and (12).

Design	H	m_1''	m_2''	f_{DW}	ϕ_R	f_R	f_R/f_{DW}	f_{01}	f_{02}
1	45	2.9	1	327	56	325	1	246	653
2	45	2.9	2	259	56	325	1.3	216	591
3	45	2.9	5.4	205	56	325	1.6	183	552
	mm	kg m^{-2}	kg m^{-2}	Hz	%	Hz	-	Hz	Hz

Accepted Manuscript

gap. In order to account for damping caused by mechanical losses in the individual leaves of the double wall as well as the sample mounting structure, artificial damping was introduced in the analytical model by means of a power attenuation coefficient γ_0 [22]. This leads to a complex speed of sound $\tilde{c}_0$ given by $1/\tilde{c}_0 = 1/c_0 - \mathrm{i}\gamma_0/(2\omega)$ which is used in Eq. (13) instead of c_0. The measurements of the double wall without Helmholtz resonators were used to estimate both, the limiting angle θ_{lim} and attenuation coefficient γ_0 for the given experimental setup. Good agreement with the measured data could be achieved with the values $\theta_{\mathrm{lim}} = 73°$ and $\gamma_0 = 0.75\ \mathrm{m}^{-1}$ which were used for all subsequent analytical calculations.

4.2. Measurement results

In the first place, measurements were conducted on the single wall, i.e. the Helmholtz resonator panel that acts on its own and is not installed in a double wall. Two configurations were measured: firstly, the panel with all the resonators active and secondly, the panel with all the necks closed by tape, such that the resonators were inactive. The measured transmission loss of the Helmholtz resonator panel was used to identify the resonance frequency f_R of the resonators and the corresponding damping ratio ζ_R. Fig. 11(a) shows the measurement results (symbols) and compares them to the analytical results (curves) which were obtained by setting $m_2'' = 0$ (i.e. no second wall). The frequency and damping ratio of the resonators were identified from the STL maximum in the measurement results as $f_R = 325$ Hz and $\zeta_R \approx 4$ %, respectively. The deviation from the previously estimated resonance frequency of 333 Hz can be attributed to the approximated end correction of the effective resonator neck length. The transmission loss of the panel with the inactive resonators (black dotted curve) was calculated using the mass law of a limp wall. The comparison of the measured and calculated transmission loss TL in Fig. 11(a) shows a good agreement for the specified parameters. The analytical model therefore can be regarded as suitable for the modelling of the Helmholtz resonator panel.

The insertion loss ΔTL with respect to the Helmholtz resonator panel with closed resonators is depicted in Fig. 11(b). The results show that the diffuse sound transmission loss is improved in a narrow frequency

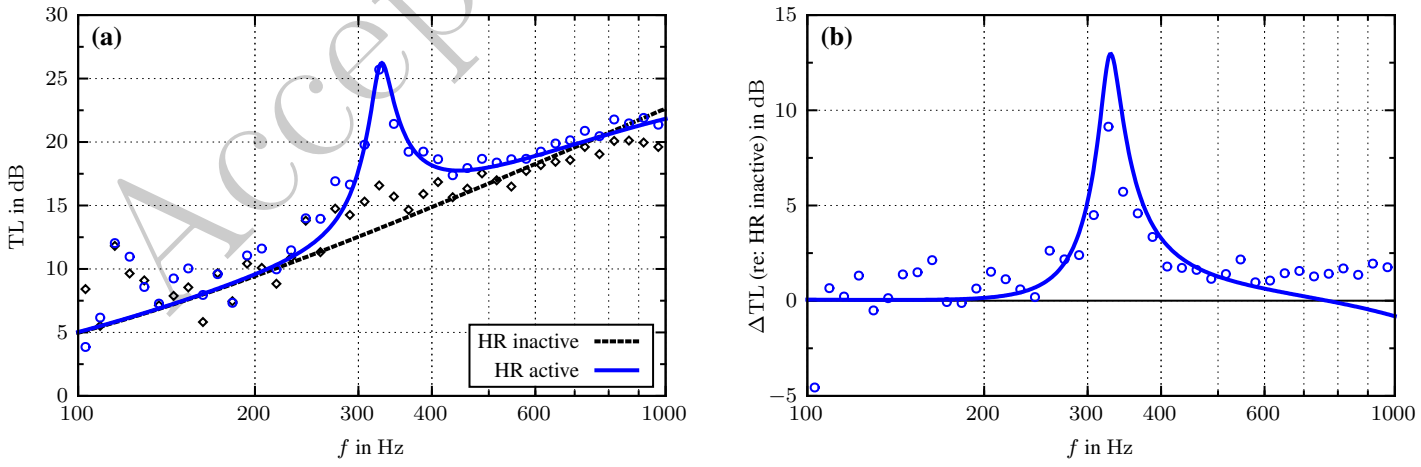

Figure 11: Comparison of experimental (symbols) and analytical results (curves) for the diffuse field sound transmission loss TL and insertion loss ΔTL (with respect to the closed Helmholtz resonators) of the Helmholtz resonator panel (single wall). (a) Transmission loss TL; (b) Insertion loss ΔTL.

Accepted Manuscript

band at the Helmholtz resonance frequency f_R by around 10 dB in the experimental data and 13 dB in the analytical calculations. The calculated insertion loss shows a negative trend in the higher frequency region. This effect is not visible in the experimental data and one possible explanation for this deviation could be the simple model in Eq. (11) for the effective density of the Helmholtz resonator. An improved model for the effective density of air volumes with Helmholtz resonators could be subject for future work. However, the use of Eq. (11) is adequate here since the focus of this paper is the frequency region around the mass-air-mass resonance frequency f_{DW} and the resonator resonance frequency f_R and not the higher frequency region.

Fig. 12(a) to (c) show the transmission loss values of the three double wall designs that are specified in Table 2. Experimental data (symbols) are compared to the analytically calculated transmission loss (curves). In all three plots, the black dotted curves and diamond symbols represent the corresponding results for the reference configurations with the same wall masses and wall spacing, but inactive Helmholtz resonators. In the analytical model, the reference configurations were calculated by setting $\phi_R = 0$. The arrows indicate the resonance frequencies of the double walls calculated for normal incidence using Eq. (12) (HR active) and Eq. (1) (HR inactive).

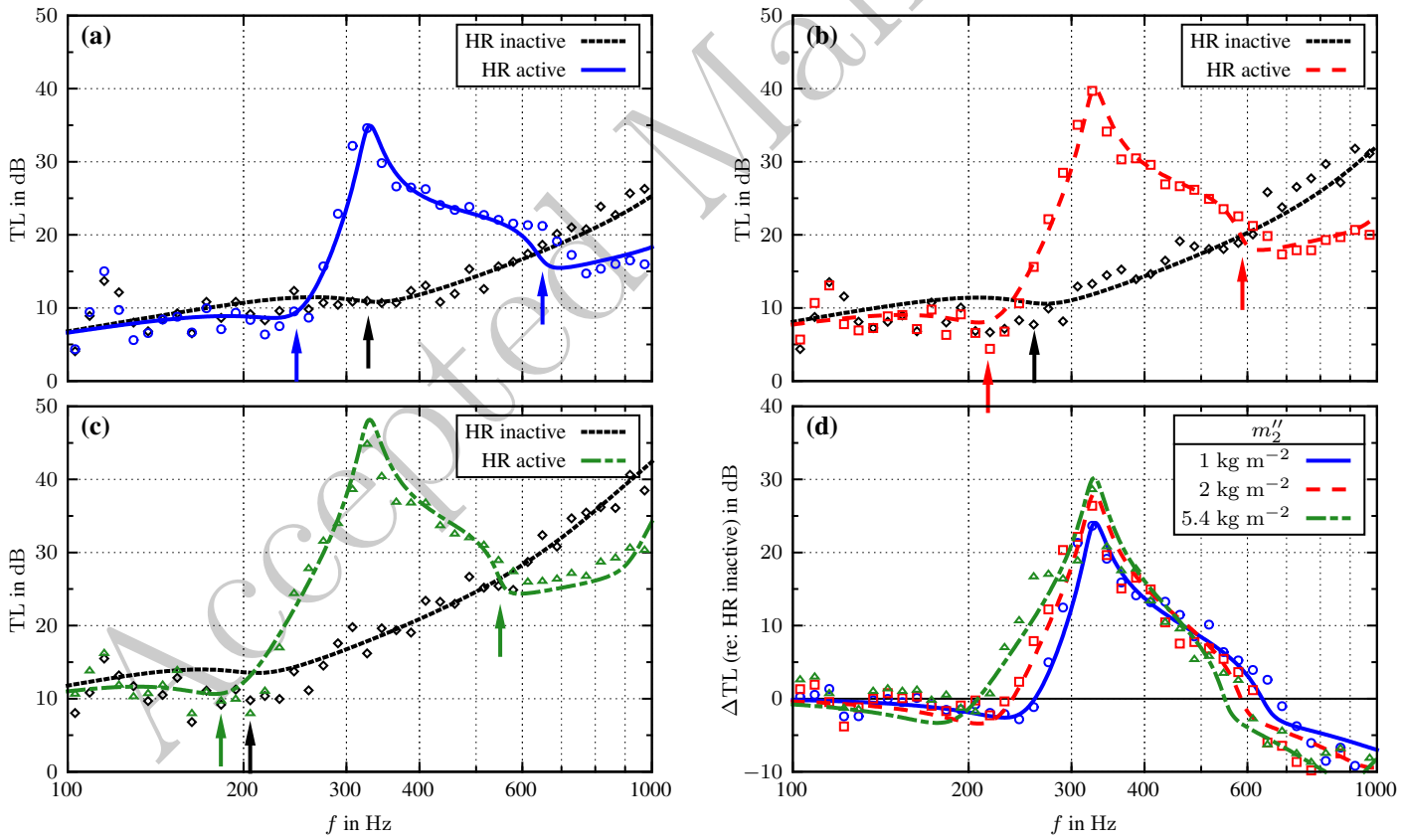

Figure 12: Comparison of experimental (symbols) and analytical results (curves) for the diffuse field sound transmission loss TL and insertion loss ΔTL of the different double wall designs with Helmholtz resonators. The arrows indicate the double wall resonance frequencies calculated for normal incidence using Eq. (12) (HR active) and Eq. (1) (HR inactive). (a) Design 1: $m_2'' = 1\,\mathrm{kg\,m^{-2}}$, $f_R/f_{\mathrm{DW}} \approx 1$; (b) Design 2: $m_2'' = 2\,\mathrm{kg\,m^{-2}}$, $f_R/f_{\mathrm{DW}} \approx 1.3$; (c) Design 3: $m_2'' = 5.4\,\mathrm{kg\,m^{-2}}$, $f_R/f_{\mathrm{DW}} \approx 1.6$; (d) Insertion loss ΔTL of the three double wall designs.

Accepted Manuscript

Overall, the experimental and analytical data show a good agreement in all of the three cases over most of the considered frequency range. This implies that, despite its simplicity, the proposed analytical model is capable of providing accurate predictions for the STL of double walls with Helmholtz resonators under diffuse incidence. The figures show that the double walls with Helmholtz resonators exhibit a broadband improvement (over one octave) of the sound transmission loss around the Helmholtz resonance frequency. From the location of the arrows it can be seen that, even though the STL results in Fig. 12 have been obtained for diffuse incidence, the normal incidence double wall resonances f_{01} and f_{02} calculated using Eq. (12) still provide a reasonably good estimate of the frequency range for the improved double wall STL.

A comparison of the insertion loss ΔTL for all three double wall designs is plotted in Fig. 12(d). It is obvious that the sound transmission loss is improved for all three designs over more than one octave with a maximum STL improvement of 25 to 30 dB (depending on the surface mass density m_2''). In contrast, the insertion loss of the Helmholtz resonator panel was narrowband and had a measured maximum value of 10 dB (see Fig. 11(b)). At this point it should be emphasized that the measured STL improvement of the double wall is remarkably large and only originates from the Helmholtz resonators inside the cavity. By choosing the specific reference configuration with the closed and shifted Helmholtz resonator panel, any influence of changed mass and/or cavity size on the double wall STL could be ruled out.

Fig. 12(d) shows clearly the influence of increasing the ratio of the resonance frequency to the mass-air-mass resonance frequency f_R/f_{DW}: The resonance frequencies f_{01} and f_{02} are shifted to lower frequencies with increasing f_R/f_{DW}. This also shifts the transmission loss improvement to lower frequencies. Calculation of the bandwidth (introduced in Section 3) reveals that the double wall design 3 with the highest value of m_2'' exhibits the highest bandwidth with about $B = 107$ % in the measurements (analytical model: 101 %). Design 1 with the lowest value of m_2'', on the other hand, has a measured bandwidth of 98 % (analytical model: 92 %). This is in line with the results from the parametric study in Section 3 where it was shown that by increasing f_R/f_{DW} the bandwidth of the STL improvement can be improved.

5. Conclusions

In this paper it was investigated how a more broadband improvement of the sound transmission loss of a double wall using Helmholtz resonators inside the cavity can be achieved. A simple analytical model was presented to describe the vibro-acoustic behavior of a double wall with Helmholtz resonators. Sound intensity measurements of different double wall designs with integrated Helmholtz resonators have been employed to validate the model and demonstrate the broadband STL improvement under diffuse field incidence. The key findings of this contribution can be summarized as follows:

- A fluid volume containing Helmholtz resonators (e.g. the cavity of a double wall with Helmholtz resonators) can be represented by a volume with equivalent fluid properties (effective bulk modulus and density) given by Eqs. (8) and (11), respectively. This representation depends only on the background fluid properties, the volumetric filling ratio ϕ_R, Helmholtz resonance frequency f_R, damping ratio ζ_R,

Accepted Manuscript

and, if applicable, the properties of the fluid inside the resonator. The analytical model can be used to calculate the resonance frequencies and sound transmission loss of a double wall with Helmholtz resonators.

- The Helmholtz resonators change the effective bulk modulus of the air cavity between the walls such that the mass-air-mass resonance frequency f_{DW} of the double wall can be significantly reduced compared to a standard double wall with the same mass and wall spacing. This shifting of f_{DW} depends only on the filling ratio and the resonance frequency ratio f_R/f_{DW}.

- The reduction of the mass-air-mass resonance frequency leads to the emergence of a frequency band with a significantly improved transmission loss. Parametric studies revealed that the bandwidth of the STL improvement can become very large for large filling ratios ϕ_R and f_R much greater or smaller than f_{DW}. The average STL improvement in this frequency band, however, becomes smaller if the Helmholtz resonance frequency and mass-air-mass frequency are too far apart.

- At higher frequencies the decoupling of the Helmholtz resonators from the rest of the double wall cavity leads to a decrease in the double wall STL. This STL reduction becomes greater when the filling ratio of the resonators is increased. Thus, there is a certain trade-off between an enhanced low-frequency STL over a wide frequency band and a reduced performance at higher frequency that needs to be taken into account in the design of double walls with Helmholtz resonators for noise control.

- Using the sound intensity measurement results of three different double wall designs the proposed analytical model could be validated. In addition to that, it could be shown that also under diffuse incidence the broadband STL improvement can be achieved with Helmholtz resonators. As in the normal incidence results, the bandwidth could be increased by increasing f_R/f_{DW}.

Practical implications of the presented results are that it could be shown that broadband STL improvement of double walls can be achieved using Helmholtz resonators. This provides a new perspective on the design of double wall partitions with Helmholtz resonators compared to previous research on this topic which mainly focused on tonal improvements and tuning of the Helmholtz resonators to frequencies very close to the mass-air-mass resonance frequency. It is, however, also important to consider the negative impact of the Helmholtz resonators at higher frequencies. Although it can be expected that due to the dominance of structure-borne sound bridges and porous absorption at higher frequencies this deterioration can be alleviated, the high frequency behavior can be of significance depending on the noise source characteristics. Furthermore, the analytical model introduced in this work provides a generalized way to represent double walls containing acoustic resonators. The model does not require geometrical details of the Helmholtz resonators and can therefore be applied in early design stages to reduce the parameter space and optimize the sound insulation of partitions.

Accepted Manuscript

Acknowledgements

This work has been performed under the framework of the research projects New Acoustic Insulation Metamaterial Technology for Aerospace (NAIMMTA), funded by the Federal Ministry of Education and Research (grant number: 03INT504AB), and Flight-LAB, funded by the Federal Ministry for Economic Affairs and Energy (grant number: 20K1511D). The financial support is gratefully acknowledged by the authors. Furthermore, the authors would like to thank Evonik for providing the foam material that was used to manufacture the Helmholtz resonator panel.

References

[1] F. J. Fahy, P. Gardonio, Sound and structural vibration: radiation, transmission and response, Academic press, Oxford, UK, 2007.

[2] N. de Melo Filho, L. V. Belle, C. Claeys, E. Deckers, W. Desmet, Dynamic mass based sound transmission loss prediction of vibro-acoustic metamaterial double panels applied to the mass-air-mass resonance, J. Sound Vib. 442 (2019) 28–44.

[3] F. Langfeldt, W. Gleine, O. von Estorff, Enhancing the low-frequency noise reduction of a double wall with membrane-type acoustic metamaterials, in: Proc. Inter-Noise 2016, Hamburg, 2016, pp. 7551–7562.

[4] J. Mason, F. Fahy, The use of acoustically tuned resonators to improve the sound transmission loss of double-panel partitions, J. Sound Vib. 124 (1988) 367–379.

[5] R. A. Prydz, L. S. Wirt, H. L. Kuntz, L. D. Pope, Transmission loss of a multilayer panel with internal tuned helmholtz resonators, J. Acoust. Soc. Am. 87 (1990) 1597–1602.

[6] S. Sugie, J. Yoshimura, T. Iwase, Effect of inserting a helmholtz resonator on sound insulation in a double-leaf partition cavity, Acoust. Sci. Technol. 30 (2009) 317–326.

[7] H. L. Kuntz, R. J. Gatineau, R. A. Prydz, F. J. Balena, Development and testing of cabin sidewall acoustic resonators for the reduction of cabin tone levels in propfan-powered aircraft, NASA CR-4388, 1991.

[8] P. Sas, C. Bao, F. Augusztinovicz, W. Desmet, Active control of sound transmission through a double panel partition, J. Sound Vib. 180 (1995) 609–625.

[9] J. P. Carneal, C. R. Fuller, Active structural acoustic control of noise transmission through double panel systems, AIAA J. 33 (1995) 618–623.

[10] I. U. Borchers, S. T. Laemmlein, P. Bartels, A. Rausch, M. Faust, J. A. F. Coebergh, K. Koeble, Acoustic protection on payload fairings of expendable launch vehicles, 1997. United States Patent No. 5,670,758.

Accepted Manuscript

[11] D. Gely, G. Elias, N. Lupoglazoff, F. Vuillot, F. Micheli, Aeroacoustic characterization and numerical simulation of a helmholtz resonator, in: Proc. 5th AIAA/CEAS Aeroacoustics Conference and Exhibit, Bellevue, WA, 1999, pp. 929–936.

[12] J. P. den Hartog, Mechanical Vibrations, 4th ed., Dover Publications, New York, 1985.

[13] I. Jordanov, B. Cheshankov, Optimal design of linear and non-linear dynamic vibration absorbers, J. Sound Vib. 123 (1988) 157–170.

[14] S. J. Estève, M. E. Johnson, Reduction of sound transmission into a circular cylindrical shell using distributed vibration absorbers and helmholtz resonators, J. Acoust. Soc. Am. 112 (2002) 2840–2848.

[15] N. Sui, X. Yan, T.-Y. Huang, J. Xu, F.-G. Yuan, Y. Jing, A lightweight yet sound-proof honeycomb acoustic metamaterial, Appl. Phys. Lett. 106 (2015) 171905.

[16] A. Peiffer, M. Grünewald, P. Lempereur, Comment on "A lightweight yet sound-proof honeycomb acoustic metamaterial" [Appl. Phys. Lett. 106, 171905 (2015)], Appl. Phys. Lett. 107 (2015) 216101.

[17] American Society for Testing and Materials ASTM E2611-09, Standard test method for measurement of normal incidence sound transmission of acoustical materials based on the transfer matrix method, 2009.

[18] D. A. Bies, C. H. Hansen, Engineering Noise Control: Theory and Practice, 4th ed., Spon Press, London, 2009.

[19] J. F. Allard, N. Atalla, Propagation of Sound in Porous Media: Modelling Sound Absorbing Materials, 2 ed., John Wiley & Sons, Chichester, 2009.

[20] J. G. Berryman, Long-wavelength propagation in composite elastic media i. spherical inclusions, J. Acoust. Soc. Am. 68 (1980) 1809–1819.

[21] Q. Mao, S. Pietrzko, Control of sound transmission through double wall partitions using optimally tuned helmholtz resonators, Acta Acust. united Ac. 91 (2005) 723–731.

[22] T. Vigran, Sound insulation of double-leaf walls – allowing for studs of finite stiffness in a transfer matrix scheme, Appl. Acoust. 71 (2010) 616–621.

Accepted Manuscript